Supporting Information

Accelerated Indirect Photolysis of UV-328 within the Hydrophobic Microdomains of Dissolved Organic Matter: The Role of Sorption and Localized Reactive Intermediates

[1]Mingzhu He[a], [1]Zhansheng Li[a], Hongxia Zhao[a,*], Yuhong Su[b,*], Shafiul Azam[a], Jiawen Shao[a]

[a] Key Laboratory of Industrial Ecology and Environmental Engineering (Ministry of Education), School of Environmental Science and Technology, Dalian University of Technology, Dalian, 116024, China

[b] College of Chemical Engineering, Petroleum and Natural Gas and Fine Chemicals Key Laboratory, Xinjiang University, Urumqi 830046, China

[*]Corresponding author.

Email: hxzhao@dlut.edu.cn (H. Zhao), 194866912@qq.com (Y. Su).

Text S1. Materials and chemicals

2-(2H-benzotriazol-2-yl)-4,6-di-tert-amylphenol (UV-328) was produced by Sigma-Aldrich (Germany). Six DOM types were used in the experiment. Humic acid (HA) and fulvic acid (FA) were purchased from Sigma-Aldrich (St. Louis, MO, USA). The other four types of DOM were purchased from the International Humic Substances Association (IHSS), including Suwannee River natural organic matter (SRNOM, 2R101N), fulvic acid (SRFA, 3S101F), Mississippi River natural organic matter (MRNOM, 1R110N), and Leonardite humic acid (LHA, 1S104H). Ultrapure water was prepared using the Milli-Q Water Purification System (≥18.2 MΩ·cm, Millipore, Bedford, USA). Chromatographic-grade dichloromethane, acetonitrile, and methanol were purchased from Sigma-Aldrich (Germany). Benzoic acid (BA), p-hydroxybenzoic Acid (p-HBA), 2,4,6-trimethylphenol (TMP), furfuryl alcohol (FFA), furfuryl alcohol derivative (furfurylamine, FFAm) were purchased from Aladdin Chemical Co., Ltd. (Shanghai, China). Sodium hydrogen phosphate, sodium dihydrogen phosphate, sodium hydroxide, and ammonium acetate were also purchased from Aladdin Chemical Co., Ltd. (Shanghai, China).

Text S2. Experimental details of solubility enhancement

The adsorption kinetics experiments of UV-328 and HA (10 and 20 mg C L^{-1}) were carried out for 6 days using the same experimental process as the solubility enhancement method. The reaction flask was kept in the dark at 25 ℃, and three samples were collected repeatedly at each time point. Fig. S1 shows that it took at least 4 days to ensure that equilibrium was reached. Due to the high hydrophobicity of UV-328, the solubility enhancement data showed a high degree of dispersion. The concentration of the compound in each reaction flask far exceeded the water solubility

of the compound, so an important source of deviation from the data point was that UV-328 detached from the container wall during the equilibrium process. To reduce the deviation of the data, outliers were removed only when they exceeded ±2 standard deviations from the mean of replicate measurements. Three replicate samples were prepared for each DOC concentration, and at least seven DOC concentrations were used to determine each K_{DOC} value. All replicate measurements for a single DOC concentration were excluded only when the mean significantly deviated from the 95% confidence interva.

Text S3. Study on spectral characteristics of DOM

Molar absorptivity at 280 nm (ε_{280}) was calculated as the UV absorbance at 280 nm normalized to the DOC concentration in mol C/L(1). The specific ultraviolet absorbance was calculated at 254 nm ($SUVA_{254}$), which is the absorbance per unit of organic carbon content(2). The fluorescence index (FI), a complementary parameter to ε_{280}, was calculated as the ratio of emission intensity at 470 nm to that at 520 nm at a fixed excitation wavelength (λ_{ex}) of 370 nm(3); the humification index (HIX) was calculated at λ_{ex} = 254 nm, dividing the total fluorescence over λ_{em} (emission wavelengths) = 435-480 nm by the total sum of fluorescence from λ_{em} = 300-345 nm and 435-480 nm; the biological index (BIX) was calculated at λ_{ex} = 310 nm as the ratio of fluorescence at λ_{em} = 380 nm to 430 nm(4).

Text S4. Photolysis contribution rate of PPRIs

$$k = k_{h\nu} + k_{\cdot OH} + k_{{}^1O_2} + k_{{}^3DOM^*} + k_{others} \#S4.1$$

The calculation formula for ·OH contribution rate:

$$\cdot OH\% = \frac{k_{\cdot OH}}{k} = 1 - \frac{k_{IPA}}{k} \#S4.2$$

The calculation formula of $^3DOM^*$ contribution rate:

$$^3DOM^*\% = \frac{k_{^3DOM^*}}{k} = 1 - \frac{k_{TMP}}{k} - \frac{k_{IPA} - k_{NaN_3}}{k} \#S4.3$$

The calculation formula of $^1O_2$ contribution rate:

$$^1O_2\% = \frac{k_{^1O_2}}{k} = 1 - \frac{k_{NaN_3}}{k} - \left(1 - \frac{k_{IPA}}{k}\right) = \frac{k_{IPA}}{k} - \frac{k_{NaN_3}}{k} \#S4.4$$

In these equations, k was the total photodegradation rate constant of UV-328; $k_{\cdot OH}$ was the reaction rate constant of ·OH and UV-328; $k_{^1O_2}$ was the reaction rate constant of $^1O_2$ and UV-328; $k_{^3DOM^*}$ was the reaction rate constant of $^3DOM^*$ and UV-328. The k_{IPA}, k_{TMP}, and k_{NaN_3} were the reaction rate constant after adding quenchers IPA, TMP, and NaN_3, respectively.

Text S5. Determination of the second-order reaction rate constant of UV-328 and PPRIs

S5.1. The second-order reaction rate constant of UV-328 with ·OH ($k_{UV-328,\cdot OH}$)

·OH was generated by the UV/H_2O_2 system. The second-order reaction rate constant of UV-328 with ·OH was determined by competition kinetics using BA as a probe. Given the pKa of BA (≈4.2), BA exists predominantly as deprotonated benzoate ion (BzO^-) under our experimental neutral pH conditions. Therefore, $k_{BzO^-,\cdot OH}$ (5.9×10^9 M^{-1} s^{-1}) was the second-order reaction rate constant for the reaction of BzO^- and ·OH(5). The concentrations of H_2O_2, UV-328, and BA in the reaction system were 5

mM, 5 μM, and 5 μM. 1 mL aliquots were taken at predetermined time intervals, and the residual H_2O_2 was immediately quenched with 20 μL of 1.0 M $Na_2S_2O_3$. The second-order rate constant $k_{UV-328,\cdot OH}$ was calculated using the following equation:

$$k_{UV-328,\cdot OH} = \frac{ln([UV-328]_t/[UV-328]_0)}{\ln([BA]_t/[BA]_0)} k_{BzO^-,\cdot OH} \#S5.1$$

S5.2. The second-order reaction rate constant of UV-328 with $^1O_2$ ($k_{UV-328,^1O_2}$)

In the molybdate/H_2O_2 catalytic system, molybdate catalyzed the disproportionation reaction of H_2O_2 to produce $^1O_2$. FFA, which had a known second-order reaction rate constant with $^1O_2$, was used as a probe to determine $k_{UV-328,^1O_2}$by competitive kinetics. The concentrations of MnO_4^{2-}, H_2O_2, UV-328 and FFA were 1 mM, 10 mM, 5 μM, respectively. At predetermined time intervals, 1 mL aliquots were transferred to a vial pre-filled with 50 μL of 10 mM histidine to quench the residual $^1O_2$. The second-order rate constant $k_{UV-328,^1O_2}$was calculated using the following equation:

$$k_{UV-328,^1O_2} = \frac{ln([UV-328]_t/[UV-328]_0)}{\ln([FFA]_t/[FFA]_0)} k_{FFA,^1O_2} \#S5.2$$

S5.3. The second-order reaction rate constant of UV-328 with $^3RB^*$ ($k_{UV-328,^3RB^*}$)

$^3DOM^*$ is an important reactive intermediate in natural water. However, due to the complex structure and large molecular weight of $^3DOM^*$, it was difficult to directly determine. Therefore, small-molecular-weight compounds with quinone and ketone chromophores were often used as model compounds. The commonly used small molecular model compounds were riboflavin (RB), sodium anthraquinone-2-sulfonate (AQ2S), 1-nitronaphthalene, etc. Compared with $^3AQ2S^*$, the energy levels and redox

potentials of $^3RB^*$ are closer to those of $^3DOM^*$(6). Therefore, in this study, RB was used as a small-molecule model compound for DOM to determine the second-order reaction rate constant for $^3RB^*$ with UV-328.

RB was excited to $^3RB^*$ upon light absorption. $^3RB^*$ can react with UV-328 and also generate $^1O_2$ via energy transfer. Therefore, it is necessary to consider the simultaneous reactions of UV-328 with both $^1O_2$ and $^3RB^*$. The reaction scheme is as follows:

$$R_{^3RB^*} = \sum_{\lambda} \frac{I_\lambda \varepsilon_\lambda^{RB}\left(1 - 10^{-\varepsilon_\lambda^{RB}[RB]l}\right)}{\varepsilon_\lambda^{RB}[RB]l}[RB]\Phi_{^3RB^*} \#S5.3$$

Here, $R_{^3RB^*}$ was the formation rate of $^3RB^*$ (M s^{-1}); $[RB]$ was the initial concentration of RB (M); ε_λ^{RB} was the molar absorption coefficient of RB at the wavelength of λ nm (cm^{-1} M^{-1}). $\Phi_{^3RB^*}$ was the quantum yield of $^3RB^*$ excited by RB after light absorption, which was 0.375(7); I_λ was the light intensity at the center of the quartz tube (einstein cm^{-2} s^{-1}) under the irradiation of a 500 W mercury lamp with a 290 nm filter. The measured value of I_λ was 3×10^{-5} using a chemical actinometer.

$$R_{UV-328} = R_{^3RB^*}\left(\frac{k_{UV-328,^3RB^*}\cdot[UV-328]}{4.2\times10^5 + k_{UV-328,^3RB^*}\cdot[UV} \right. \quad S5.4$$

Here, R_{UV-328} is the initial degradation rate constant of UV-328 (M^{-1} s^{-1}); 4.2×10^5 s^{-1} is the quenching rate constant of $^3RB^*$ under aerobic conditions; 1.5×10^5 s^{-1} is the quenching rate of $^3RB^*$ under anaerobic conditions. The difference between them represents the quenching rate constant for the reaction of $^3RB^*$ with ground-state O_2

(2.7×10^5 s^{-1}). 2.5×10^5 s^{-1} is the thermal inactivation rate of $^1O_2$(8).

Text S6. Molecular probe experiment

S6.1. ·OH

BA was used as a molecular probe to determine the steady-state concentration of ·OH ($[\cdot OH]_{ss}$) in the reaction system by measuring the rate at which BA reacted with ·OH to form p-hydroxybenzoic acid (p-HBA). BA was added to a 10 mg C L^{-1} DOM solution at an initial concentration of 0.5 mM. After a period of illumination, samples were taken at regular intervals and passed through a 0.22 μm nylon membrane filter for HPLC analysis. The formation rate of p-HBA (R_{p-HBA}) and the formation rate of ·OH ($R_{\cdot OH}$) were obtained from the following equation, and the conversion factor between them was 5.87 ± 0.18(9).

$$R_{\cdot OH} = R_{p-HBA} \cdot 5.87 \#S6.1$$

$[\cdot OH]_{ss}$was calculated using the following equation:

$$[\cdot OH]_{ss} = \frac{R_{\cdot OH}}{k_{BA^-,\cdot OH} \cdot [BA]} \#S6.2$$

Here, [BA] was the initial concentration of benzoic acid (M).

S6.2. ^{3}DOM*

The steady-state concentration of ^{3}DOM* ($[^3DOM^*]_{ss}$) was determined using TMP as the probe molecule. TMP was added to a 10 mg C L^{-1} DOM solution at an initial concentration of 100 μM. After regular sampling, the samples were passed through a 0.22 μm glass fiber filter for HPLC analysis. Although TMP can also react with $^1O_2$ and ·OH, the contribution of $^1O_2$ and ·OH to TMP conversion was negligible(10, 11).

The formation rate of $^3DOM^*$ ($R_{^3DOM^*}$) could be obtained from the following equation:

$$R_{^3DOM^*} = R_{TMP} \cdot \frac{S_{^3DOM^*} + k_{TMP,^3DOM^*} \cdot [TMP]}{k_{TMP,^3DOM^*} \cdot [TMP]} \#S6.3$$

Here, $[TMP]$ was the initial concentration of TMP (M), R_{TMP} was the initial degradation rate of TMP (M s^{-1}), $k_{TMP,^3DOM^*}$ was the second-order reaction rate constant for the reaction of TMP and $^3DOM^*$ (8.1×10^8 M^{-1} s^{-1}), $S_{^3DOM^*}$ (3.1×10^5 s^{-1}) was the sum of the rate constant for the reaction of $^3DOM^*$ with ground-state dissolved oxygen (2.2×10^5 s^{-1}) and the quenching rate constant of $^3DOM^*$ (9.0×10^4 s^{-1}) caused by other factors(12).

$[^3DOM^*]_{ss}$ was calculated using the following equation:

$$[^3DOM^*]_{ss} = \frac{R_{^3DOM^*}}{S_{^3DOM^*} + k_{TMP,^3DOM^*} \cdot [TMP]} \#S6.4$$

S6.3. $^1O_2$

The results of Cheng et al(13) showed that in the pH range of 4-8, due to an increase in the proportion of deprotonated carboxylic acid and phenolic groups, the charge density of DOM increased. The deprotonation of these groups led to an increase in the surface potential of DOM, which attracted more FFAm to accumulate near DOM, and the concentration of FFAm near DOM gradually increased. However, when the pH was further increased to 8-9, the proportion of neutral FFAm increased, resulting in a decrease in FFAm concentration near DOM. Therefore, in order to accumulate more FFAm near the DOM, the pH was maintained at 8 in this experiment. FFA and FFAm were dissolved in water to prepare a 50 mM stock solution. A 100 mM buffer salt solution with pH=8 was prepared using sodium dihydrogen phosphate and disodium

hydrogen phosphate. A 10 mg C L^{-1} DOM solution was prepared in 10 mM phosphate buffer, containing 100 μM FFA or FFAm. After regular sampling, the samples were passed through a 0.22 μm glass fiber filter for HPLC analysis. The apparent concentration of $^1O_2$ ($[^1O_2]_{app}$) measured by FFA and FFAm was calculated using the following equation:

$$[^1O_2]_{app}^{FFA} = \frac{k_{obs}^{FFA}}{k_{rxn}^{FFA}} \#S6.5$$

$$[^1O_2]_{app}^{FFAm} = \frac{k_{obs}^{FFAm}}{k_{rxn}^{FFAm}} \#S6.6$$

Here, k_{obs}^{FFA} and k_{obs}^{FFAm} were the photolysis rate constants of FFA and FFAm (s^{-1}), k_{rxn}^{FFA} was the second-order reaction rate constant for the reaction of FFA and $^1O_2$ (1.0×10^8 M^{-1} s^{-1})(14), and k_{rxn}^{FFAm} was the second-order reaction rate constant of FFAm and $^1O_2$, which was calculated using the following equation:

$$k_{rxn}^{FFAm} = \frac{1}{1+10^{(pH-pKa)}} \cdot k_{rxn}^{FFAm^+} + \frac{10^{(pH-pKa)}}{1+10^{(pH-pKa)}} \cdot k_{rxn}^{FFAm^0} \#S6.7$$

Here, pKa was the dissociation constant of FFAm (9.01 ± 0.07), $k_{rxn}^{FFAm^+}$ was the second-order reaction rate constant for the reaction of $FFAm^+$ with $^1O_2$ (4.32×10^7 M^{-1} s^{-1}), and $k_{rxn}^{FFAm^0}$ was the second-order reaction rate constant for the reaction of $FFAm^0$ with $^1O_2$ (2.07×10^8 M^{-1} s^{-1})(13).

Text S7. Indirect photolysis rate constants induced by free and bound PPRIs

When DOM and UV-328 coexist in the reaction system, competitive light absorption occurs between them, and inhibiting direct photolysis of the target. The

direct photolysis rate constant of the target in the DOM solution can be corrected using the light screening factor S_λ. S_λ can be calculated using the following equation(15):

$$S_\lambda = \frac{\left(1 - 10^{-\alpha_\lambda \times l}\right)}{2.303 \times \alpha_\lambda \times l} \#S7.1$$

Here, α_λ(cm^{-1}) was the beam attenuation coefficient (the absorbance of DOM at wavelength λ with a 1 cm path length); l (cm) was the optical path of the quartz photolysis tube receiving light, and which was 2.3 cm in this study. α_λ could be obtained by measuring the absorbance (A) of the corresponding wavelength (λm) at the wavelength of maximum specific light absorption (I^{abs}_λ). The calculation method of I^{abs}_λ was as follows: 2.3 × light intensity at a specific wavelength × molar absorption coefficient at a specific wavelength(16). Since the measured light intensities were relative, only the relative I^{abs}_λ (I'^{abs}_λ) was calculated. As shown in Fig. S8, the wavelength maximum λ_m corresponding to I'^{abs}_λ was 297 nm. The screening coefficient S_λ was calculated by using the absorbance of DOM at this wavelength.

Based on S_λ for DOM-UV-328 solutions, the indirect photodegradation rate constant k_{ind} of UV-328 initiated by DOM can be calculated(17)：

$$k_{ind} = k_{obs(with-DOM)} - k_d \times S_\lambda \#S7.2$$

In the equation, $k_{obs(with-DOM)}$ was the apparent photodegradation rate constant (h^{-1}) of UV-328 in the DOM solution, and k_d was the direct photodegradation rate constan of UV-328. k_{ind} can also be expressed as follows:

$$k_{ind} = k_{UV-328,\cdot OH}[\cdot OH]_{free,\ ss} + k_{UV-328,\cdot OH}[\cdot OH]_l + k_{UV-328,{}^1O_2}\left[{}^1O_2\right]_{bonded,ss} + k_{UV-328,{}^3RB^*}\left[{}^3DOM^*\right]_{free,ss} \quad S7.3$$

Here, $[RIs]_{free,\ ss}$ was the steady-state concentration of free PPRIs, $[RIs]_{bonded,\ ss}$ was the steady-state concentration of bound PPRIs, $k_{UV-328,\cdot OH}$, $k_{UV-328,{}^1O_2}$, and $k_{UV-328,{}^3RB^*}$ were the second-order reaction rate constants for the reactions of UV-328 with PPRIs.

Text S8. Analysis method

The quantification of pollutants and other substances was performed by high-performance liquid chromatography (HPLC, Shimadzu, Japan). The SB-C18 chromatographic column (particle size 5 μm, 2.1 mm × 150 mm, Agilent, USA) was selected. The chromatographic conditions are summarized in Table S2.

UV-328 and its photoconversion products were determined by high-performance liquid chromatography–tandem mass spectrometry (HPLC-MS/MS, Q Exactive Plus, USA). Electrospray ionization (ESI) was performed in positive ion mode, and the mass scan range was 60-1000 Da. In the experiment, the Hypersil GOLD C18 column was used as the chromatographic column, and its specification was 150 mm long, 2.1 mm inner diameter, and the filling particle size was 3 μm. The mobile phase consisted of ultrapure water and methanol. The flow rate was controlled at 0.2 mL/min. The injection volume was 10 μL. This ensured the accuracy and repeatability of the analysis. A gradient elution procedure was used to achieve effective separation of different components. From 0 to 20 min, the methanol percentage gradually increased from 0% to 80%, and then the proportion of methanol was maintained at 5% for 20-25 min to

further optimize the separation effect. In the next critical stage, the methanol ratio increased rapidly from 5% to 80%, covering 25 to 26 min to achieve complete elution of the target compounds. In the last 25-35 min, the methanol ratio was maintained at 80%, to ensure complete elution and obtain clean chromatograms for subsequent analysis. Through such a gradient elution strategy, various components in the sample were effectively separated and identified. Data acquisition and processing were performed using Xcalibur software.

Table S1. Brief information of pollutants

Compounds	Abbreviations	CAS	Structural formula	pKa	logKow
2-(2H-benzotriazol-2-yl)-4,6-di-tert-amylphenol	UV-328	21615-49-6	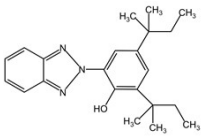	8.59	7.25

Table S2. Analysis conditions of liquid chromatography

Name	Flow phase and proportion	Wavelength (nm)	Flow velocity (mL/min)	Sample marking size (μL)
UV-328	Water:Acetonitrile (0:100)	345	1.5	10
TMP	Water:Acetonitrile (40:60)	205	1.0	30
p-HBA	1‰ Acetic acid water:Methanol (40:60)	205	1.0	30
FFA	0.025 mM Ammonium acetate: Acetonitrile (75:25)	219	1.0	50
FFAm	0.025 mMAmmonium acetate: Acetonitrile (75:25)	219	1.0	50

Table S3. Calculated values of $k_{UV-328,RI_s}[RIs]_{ss}$ for UV-328 in different DOM solutions (aqueous phase and hydrophobic microdomain)

$k_{UV-328,RI_s}[RIs]_{ss}$	HA	FA	SRNOM
$k_{UV-328,\cdot OH}[\cdot OH]_{free,ss}$	(4.37±0.20)×10^{-8}	(2.75±0.12)×10^{-8}	(2.22±0.16)×10^{-8}
$k_{UV-328,\cdot OH}[\cdot OH]_{bonded,ss}$	(4.37±0.20)×10^{-6}	(2.75±0.12)×10^{-6}	(2.22±0.16)×10^{-6}
$k_{UV-328,{}^1O_2}[{}^1O_2]_{free,ss}$	(2.02±0.11)×10^{-5}	(1.33±0.10)×10^{-5}	(0.71±0.34)×10^{-5}
$k_{UV-328,{}^1O_2}[{}^1O_2]_{bonded,ss}$	(2.02±0.11)×10^{-3}	(1.33±0.10)×10^{-3}	(0.71±0.34)×10^{-3}
$k_{UV-328,{}^3RB*}[{}^3DOM^*]_{free,ss}$	(1.44±0.11)×10^{-4}	(8.34±0.66)×10^{-5}	(4.79±0.36)×10^{-5}
$k_{UV-328,{}^3RB*}[{}^3DOM^*]_{bondea}$	(1.44±0.11)×10^{-2}	(8.34±0.66)×10^{-3}	(4.79±0.36)×10^{-3}

Table S4. UV-328 photolysis product information

Products	RT (min)	Precise mass ((M+H)+ m/z)	Measured mass ((M+H)+ m/z)	Molecular formula	Structural formula
UV-328	12.90	352.2383	352.2399	$C_{22}H_{29}N_3O$	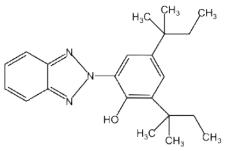
P250	18.32	251.2005	251.2001	$C_{16}H_{26}O_2$	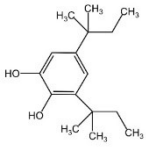
P353	13.49	354.2176	354.2144	$C_{21}H_{27}N_3O_2$	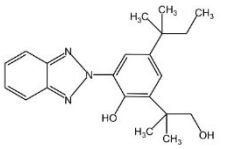
P281	17.66	282.1600	282.1591	$C_{17}H_{19}N_3O$	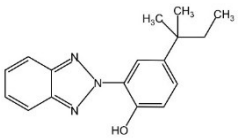
P211	7.83	212.0818	212.0799	$C_{12}H_9N_3O$	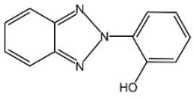

P133	1.56	134.0713	134.0711	$C_7H_7N_3$	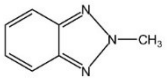
P119	4.39	120.0556	120.0554	$C_6H_5N_3$	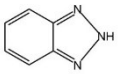
P367	3.61	368.2332	368.2302	$C_{22}H_{29}N_3O_2$	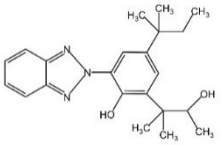
	6.02	368.2332	368.2290		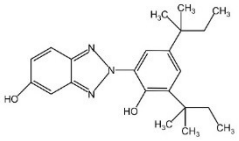
P383	6.96	384.2281	384.2246	$C_{22}H_{29}N_3O_3$	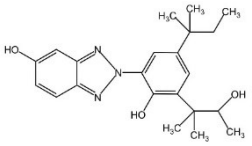
	8.96	384.2281	384.2318		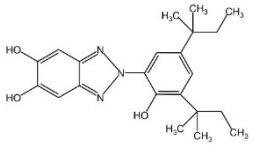
P417	14.23	418.2336	418.2311	$C_{22}H_{31}N_3O_5$	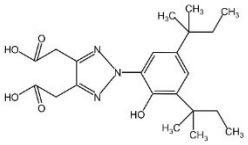
P369	1.44	370.2489	370.2452	$C_{22}H_{31}N_3O_2$	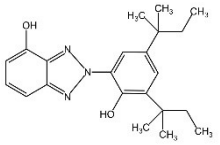

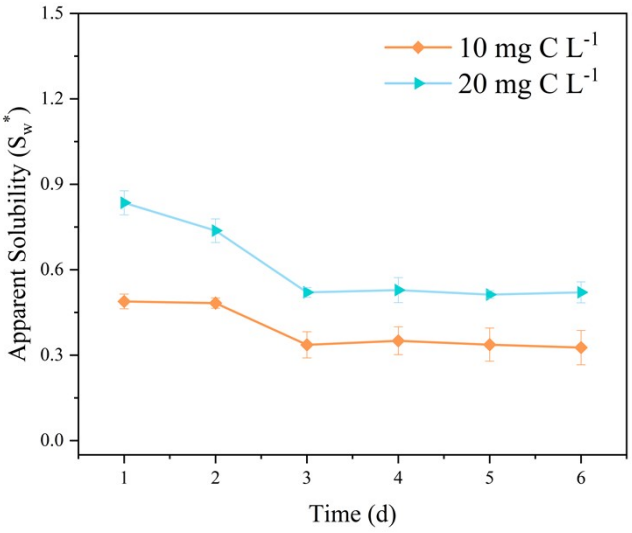

Fig. S1. Equilibrium Kinetics of UV-328 in HA-H_2O System.

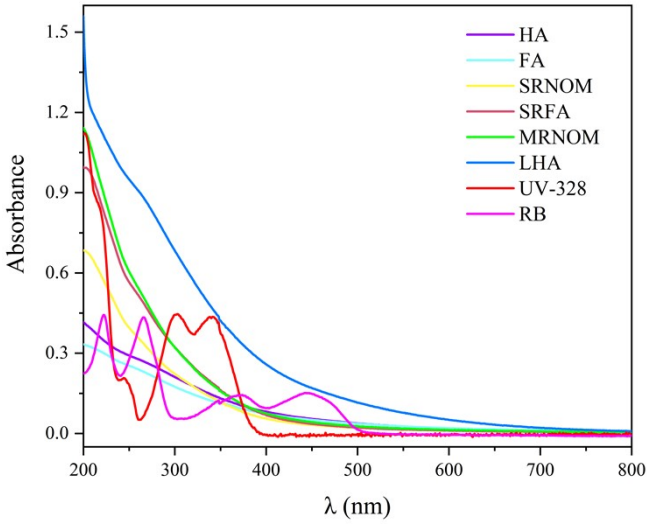

Fig. S2. UV-visible absorption spectra of UV-328 (spectra multiplied by a factor of 5 for clarity), DOM and RB.

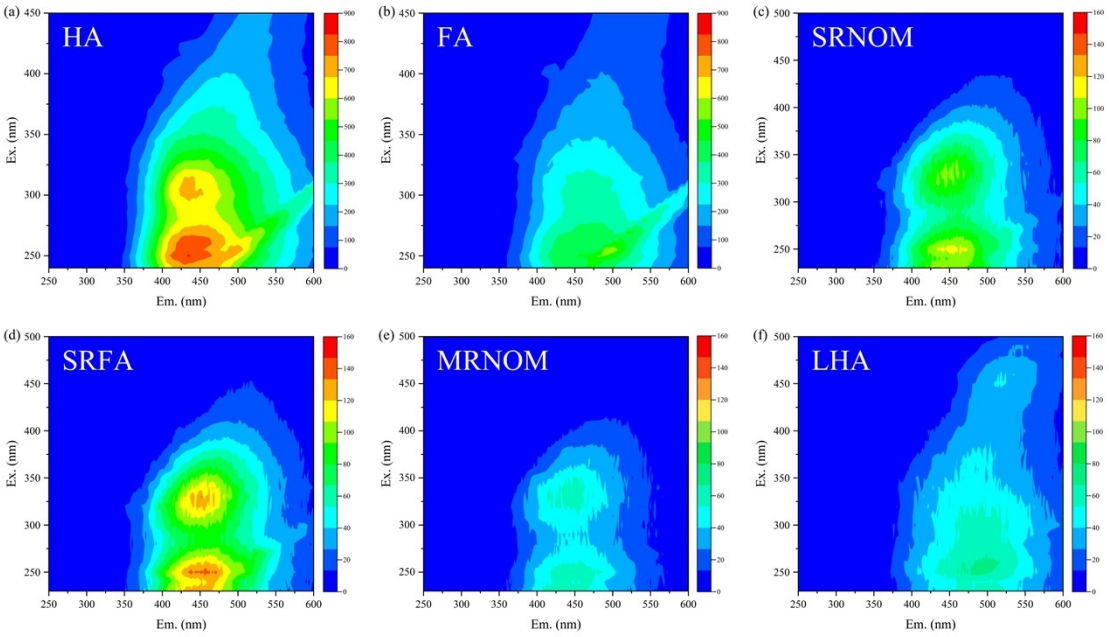

Fig. S3. Three-dimensional fluorescence spectra of DOM.

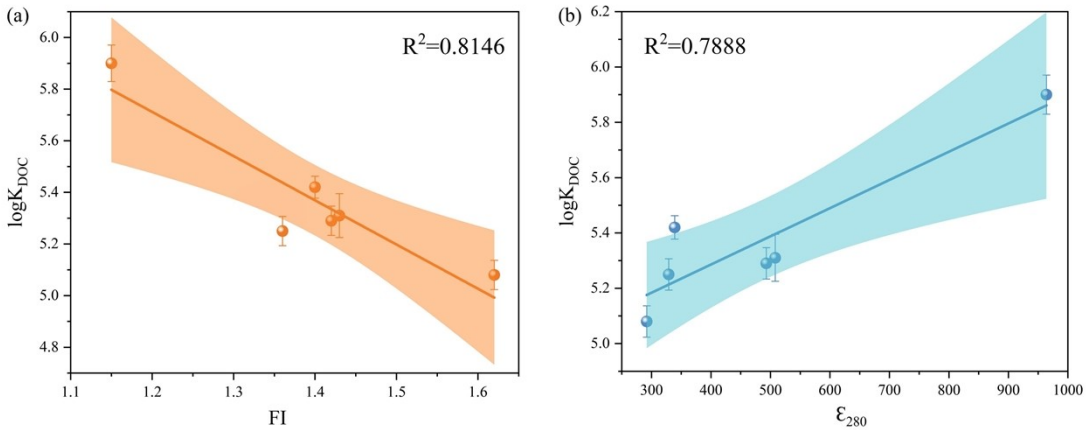

Fig. S4. The linear fitting of the measured value of $\log K_{DOC}$ with FI and ε_{280}.

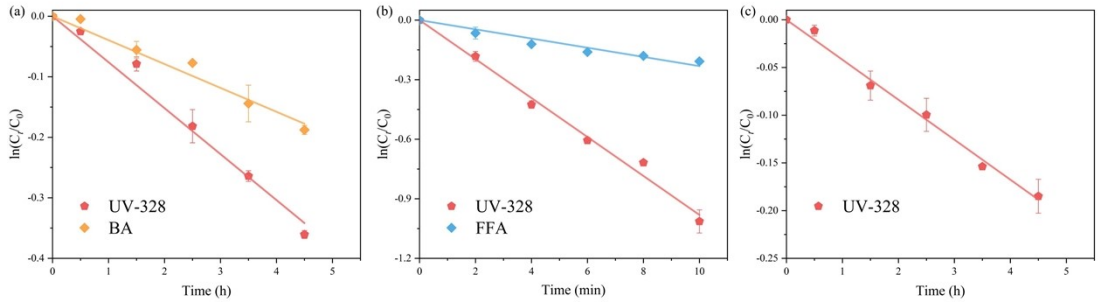

Fig. S5. (a) The second-order rate constant of UV-328 with ·OH was determined by the competition kinetics method in the H_2O_2/UV system; (b) Molybdate/H_2O_2 catalytic system produced $^1O_2$, and the second-order rate constant for the reaction of UV-328 and $^1O_2$ was determined using competition kinetics; (c) The second-order rate constants of UV-328 and $^3RB^*$ were determined using RB as a DOM model compound.

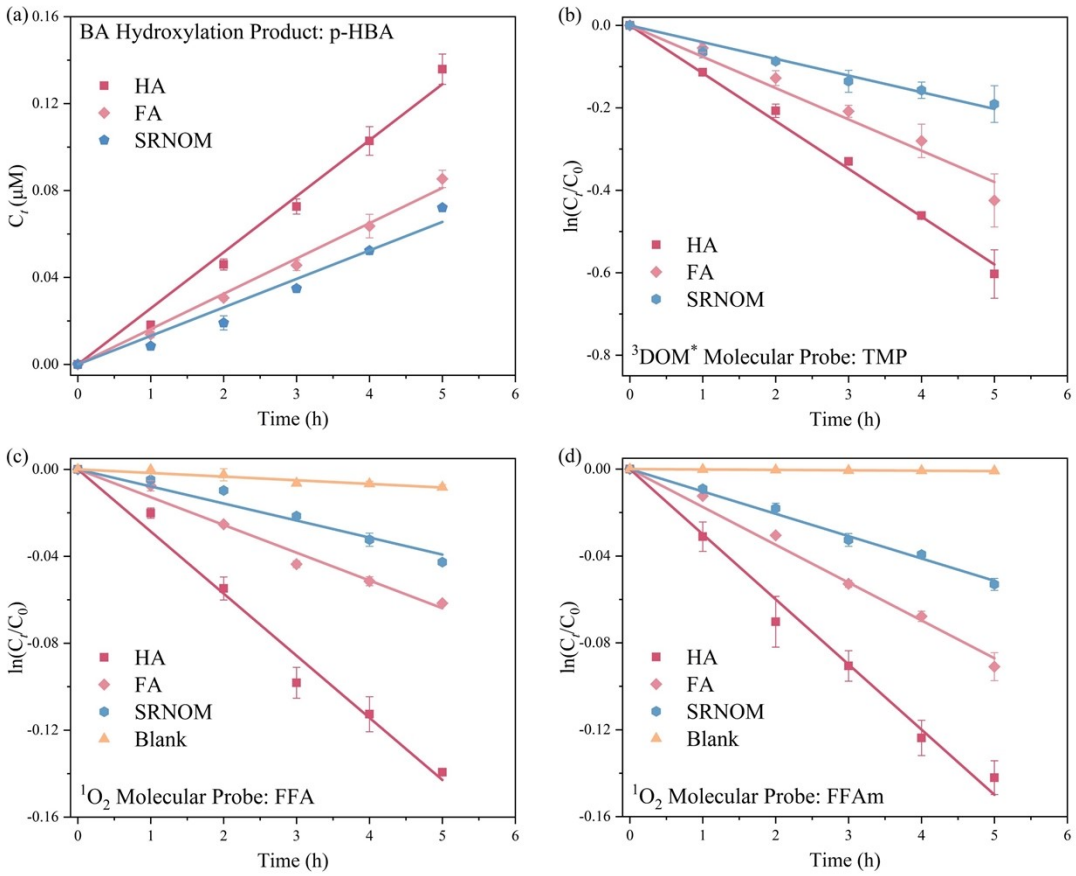

Fig. S6. (a) BA was used as a probe to determine the steady-state concentration of ·OH; (b) TMP was used as a probe to measure the steady-state concentration of ^{3}DOM*; (c) FFA was used as a probe to determine the steady-state concentration of $^1O_2$; (d) FFAm was used as a probe to determine the steady-state concentration of $^1O_2$. (DOM concentration: 10 mg C L^{-1}.)

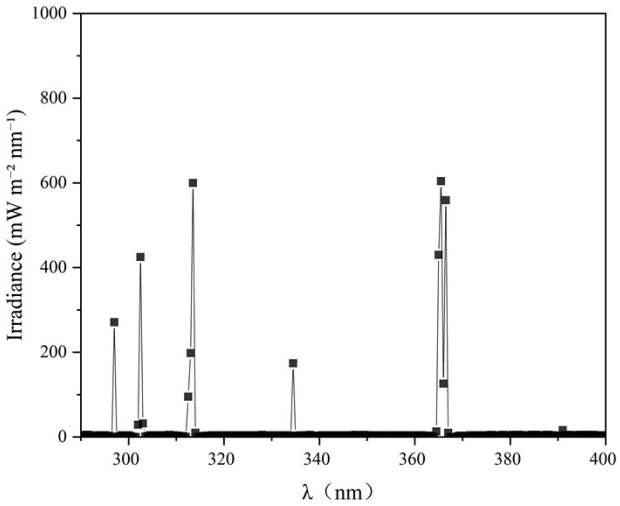

Fig. S7. Emission spectrum of the mercury lamp used in the photolysis experiments, recorded over the wavelength range 290-400 nm.

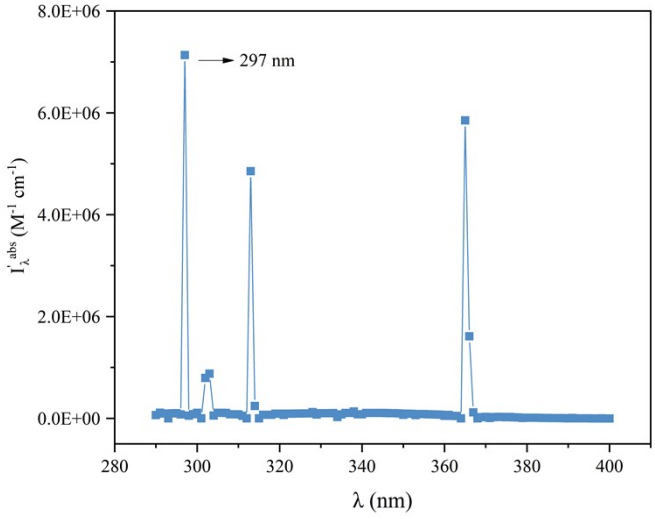

Fig. S8. Relative specific light absorption rate of UV-328 in water.

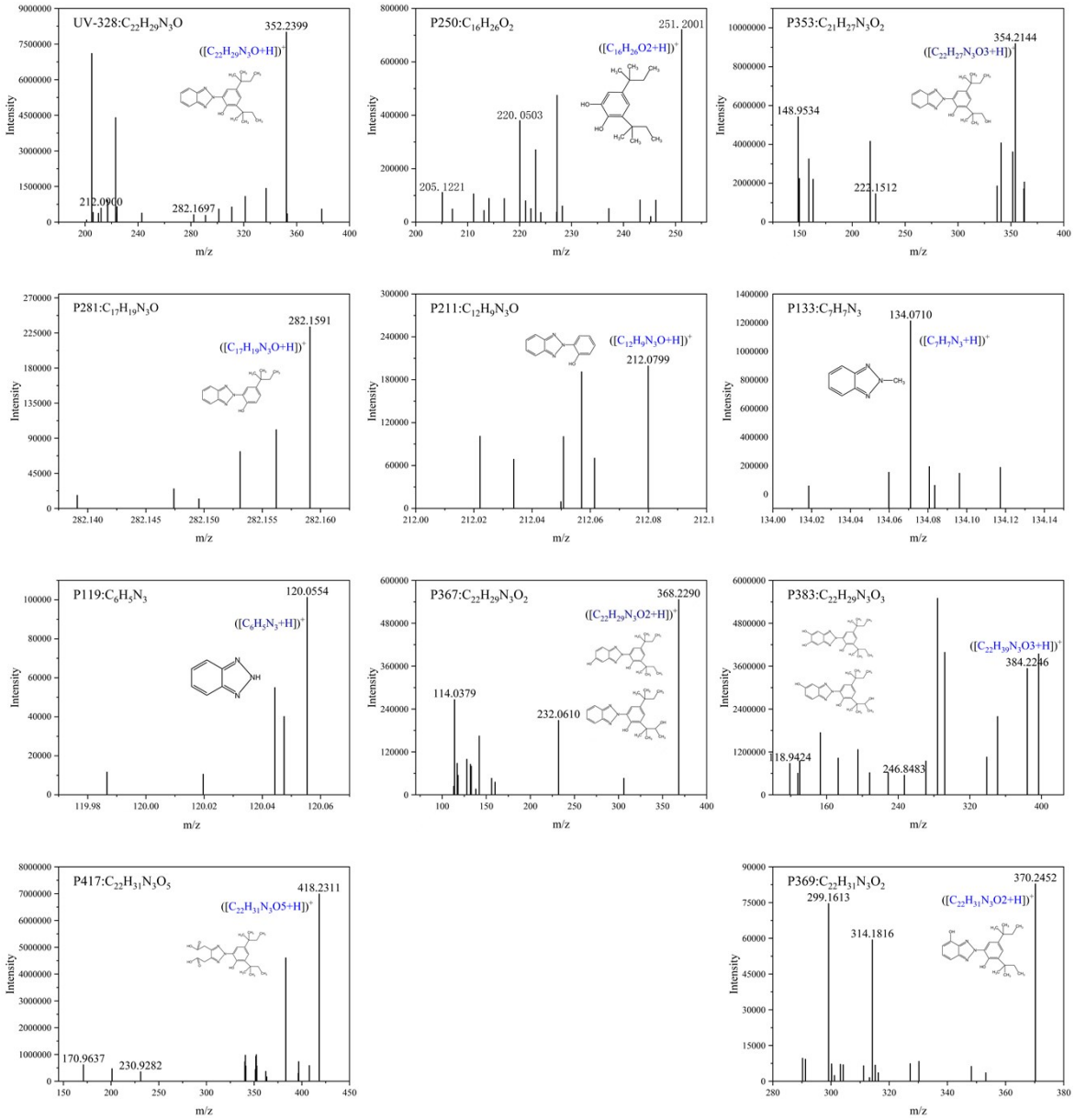

Fig. S9. Mass spectrum of photodegradation products.

References

1. Wei-Haas ML, Hageman KJ, Chin YP. Partitioning of polybrominated diphenyl ethers to dissolved organic matter isolated from Arctic surface waters. Environ Sci Technol. 2014;48(9):4852-9.
2. Weishaar JL, Aiken GR, Bergamaschi BA, Fram MS, Fujii R, Mopper K. Evaluation of specific ultraviolet absorbance as an indicator of the chemical composition and reactivity of dissolved organic carbon. Environ Sci Technol. 2003;37(20):4702-8.
3. McKnight DM, Boyer EW, Westerhoff PK, Doran PT, Kulbe T, Andersen DT. Spectrofluorometric characterization of dissolved organic matter for indication of precursor organic material and aromaticity. Limnol Oceanogr. 2001;46(1):38-48.
4. Huguet A, Vacher L, Relexans S, Saubusse S, Froidefond JM, Parlanti E. Properties of fluorescent dissolved organic matter in the Gironde Estuary. Org Geochem. 2009;40(6):706-19.
5. Buxton GV, Greenstock CL, Helman WP, Ross AB. Critical-review of rate constants for reactions of hydrated electrons, hydrogen-atoms and hydroxyl radicals (.OH/.O-) in aqueous-solution. Journal of Physical and Chemical Reference Data. 1988;17(2):513-886.
6. Bianco A, Fabbri D, Minella M, Brigante M, Mailhot G, Maurino V, et al. Photochemical transformation of benzotriazole, relevant to sunlit surface waters: Assessing the possible role of triplet-sensitised processes. Sci Total Environ. 2016;566:712-21.
7. Isiam SDM, Penzkofer A, Hegemann P. Quantum yield of triplet formation of riboflavin in aqueous solution and of flavin mononucleotide bound to the LOV1 domain of Phot1 from Chlamydomonas reinhardtii. Chem Phys (Netherlands). 2003;291(1):97-114.
8. Zhou CZ, Chen JW, Xie HJ, Zhang YN, Li YJ, Wang Y, et al. Modeling photodegradation kinetics of organic micropollutants in water bodies: A case of the Yellow River estuary. J Hazard Mater. 2018;349:60-7.
9. Zhou XL, Mopper K. Determination of photochemically produced hydroxyl radicals in seawater and fresh-water. Mar Chem. 1990;30(1-3):71-88.
10. De Laurentiis E, Buoso S, Maurino V, Minero C, Vione D. Optical and photochemical characterization of chromophoric dissolved organic matter from lakes in Terra Nova bay, Antarctica. Evidence of considerable photoreactivity in an extreme environment. Environ Sci Technol. 2013;47(24):14089-98.
11. De Laurentiis E, Minella M, Maurino V, Minero C, Brigante M, Mailhot G, et al. Photochemical production of organic matter triplet states in water samples from mountain lakes, located below or above the tree line. Chemosphere. 2012;88(10):1208-13.
12. Erickson PR, Moor KJ, Werner JJ, Latch DE, Arnold WA, McNeill K. Singlet oxygen phosphorescence as a probe for triplet-state dissolved organic matter reactivity. Environ Sci Technol. 2018;52(16):9170-8.
13. Cheng K, Zhang LZ, McKay G. Evaluating the microheterogeneous distribution of photochemically generated singlet oxygen using furfuryl amine. Environ Sci Technol. 2023;57(19):7568-77.
14. Appiani E, Ossola R, Latch DE, Erickson PR, McNeill K. Aqueous singlet oxygen reaction kinetics of furfuryl alcohol: effect of temperature, pH, and salt content. Environmental Science-Processes & Impacts. 2017;19(4):507-16.
15. Miller PL, Chin YP. Photoinduced degradation of carbaryl in a wetland surface water. J Agric Food Chem. 2002;50(23):6758-65.
16. Leal JF, Esteves VI, Santos EBH. BDE-209: Kinetic studies and effect of humic substances on photodegradation in water. Environ Sci Technol. 2013;47(24):14010-7.
17. Zhang YN, Wang JQ, Chen JW, Zhou CZ, Xie Q. Phototransformation of 2,3-dibromopropyl-

2,4,6-tribromophenyl ether (DPTE) in natural waters: Important roles of dissolved organic matter and chloride ion. Environ Sci Technol. 2018;52(18):10490-9.